Journal of Biotechnology 240 (2016) 1–13

Journal of Biotechnology

journal homepage: www.elsevier.com/locate/jbiotec

Modeling the competition between antenna size mutant and wild type microalgae in outdoor mass culture

Tim de Mooij[a,*,1], Kira Schediwy[a,1], René H. Wijffels[a,b], Marcel Janssen[a]

[a] Bioprocess Engineering, AlgaePARC, Wageningen University, PO box 16, 6700 AA, Wageningen, The Netherlands
[b] Biosciences and Aquaculture, Nord University, Bodø, 8049, Norway

ARTICLE INFO

Article history:
Received 13 June 2016
Received in revised form 10 October 2016
Accepted 12 October 2016
Available online 13 October 2016

Keywords:
Antenna size mutant
Competition
Chlorella sorokiniana
Areal biomass productivity
Photosynthetic efficiency

ABSTRACT

Under high light conditions, microalgae are oversaturated with light which significantly reduces the light use efficiency. Microalgae with a reduced pigment content, antenna size mutants, have been proposed as a potential solution to increase the light use efficiency. The goal of this study was to investigate the competition between antenna size mutants and wild type microalgae in mass cultures. Using a kinetic model and literature-derived experimental data from wild type *Chlorella sorokiniana*, the productivity and competition of wild type cells and antenna size mutants were simulated. Cultivation was simulated in an outdoor microalgal raceway pond production system which was assumed to be limited by light only. Light conditions were based on a Mediterranean location (Tunisia) and a more temperate location (the Netherlands). Several wild type contamination levels were simulated in each mutant culture separately to predict the effect on the productivity over the cultivation time of a hypothetical summer season of 100 days. The simulations demonstrate a good potential of antenna size reduction to increase the biomass productivity of microalgal cultures. However, it was also found that after a contamination with wild type cells the mutant cultures will be rapidly overgrown resulting in productivity loss.

1. Introduction

One of the most important bottlenecks in microalgae cultivation is the inefficient utilization of light energy under high irradiance. Microalgae are easily oversaturated with light which strongly reduces the light use efficiency. This limitation can be alleviated by genetically reducing the amount of light energy that is absorbed per cell. The creation of such antenna size mutants, i.e., microalgae with a reduced pigment content, has been proposed as a potential solution (Formighieri et al., 2012; Kwon et al., 2013; Mussgnug et al., 2007a; Oey et al., 2013; Ort et al., 2011; Perrine et al., 2012) to light saturation. The lower pigmentation of the mutants allows increased biomass concentrations with the same light gradient in the photobioreactor (Melis et al., 1998; Mussgnug et al., 2007b). The lower biomass specific light absorption rate leads to a higher productivity of mutant cultures than that of wild type cultures under high light conditions (Mussgnug et al., 2007b). In practice, some mutants were indeed reported to demonstrate improved growth characteristics under specific light conditions (Mussgnug et al., 2007b; Cazzaniga et al., 2014; Mitra and Melis, 2008).

Clearly, antenna size mutant generation, especially through directed mutagenesis, is an immature technology (de Mooij et al., 2014). Currently there are no suitable antenna size mutant strains available that can be analyzed for their performance in competition experiments. A better understanding of the photosynthetic machinery and an advanced genetic toolbox are required to create better mutants. Still, it is interesting to study the potential of antenna size reduction for mass cultivation of microalgae using model simulations. Extrapolation of laboratory data utilizing a predictive model that is constructed on a solid theoretical foundation is an attractive alternative to performing outdoor cultivation experiments. Modeling can function as a great tool to investigate the improvement of mass culture productivity using antenna size mutants. In addition, the impact of competition for light between mutant and wild type strains can be predicted. Competition between the antenna size mutant and its own wild type is expected to result in productivity losses. The outcome of such a modeling approach results in more realistic expectations and can be used to determine genetic engineering targets to optimize mutant cultivation.

* Corresponding author.
E-mail address: timdemooij@gmail.com (T. de Mooij).
[1] These authors contributed equally to this work.

http://dx.doi.org/10.1016/j.jbiotec.2016.10.009

The aim of this study was to estimate antenna size mutant productivity in photobioreactor mass cultures and quantify the competition between the antenna size mutant and its wild type. Knowledge on growth properties of separate cultures (Hobson, 1969; Huisman et al., 1999) is required to analyze mixed cultures and to estimate the competitiveness of the involved species under light limiting conditions. Many models describing biomass productivity of microalgae are available to date (Acién Fernández et al., 1998; Cornet and Dussap, 2009; Geider et al., 1997; Huesemann et al., 2016; Lee et al., 2014; Quinn et al., 2011; Takache et al., 2012). These models differ by their level of complexity, model strategy and need for parameterization. In our study the productivity was calculated with a microalgal growth model which is based on summing up local rates of photosynthesis calculated for every position in the photobioreactor. The presented model takes into account the light gradient within the microalgal culture and also the wavelength dependency of light absorption. The model is based on a previously validated growth model for *Chlorella sorokiniana* under continuous light (Blanken et al., 2016), that was obtained by combining models of Jassby and Platt (1976) and Pirt (1965) and the Lambert-Beer law. The model has been modified by adding a carbon partitioning mechanism and simulated outdoor light conditions to describe growth under day/night cycles. By extending the model, it serves well to answer new research questions regarding the competition of microalgae strains that have different light harvesting capacities. The light model was further adapted to represent an outdoor microalgal raceway pond production system taking into account solar elevation. The wild type properties were defined based on experimental data of *C. sorokiniana*. Antenna size mutants were considered to only differ from the wild type in their reduced absorption cross section to clearly identify the potential of reduced antenna sizes. Productivities of the mutant monocultures with different antenna size reductions (0–90%) were investigated. Several wild type contamination levels were separately simulated in each mutant culture to predict the effect on the productivity over the cultivation time (100 days).

2. Model description

2.1. Structure

With the kinetic model the biomass productivity of a microalgae mass culture is calculated as a function of the incident light intensity during the diurnal cycle. The change of the spectral composition with increasing reactor depth due to the preferential light absorption of microalgae was taken into account. The model allows for the calculation of biomass productivity of an antenna size mutant culture before, during, and after contamination with its wild type. In all of the cases, light is assumed to be the limiting factor for growth and, consequently, mutant and wild type are competing for light energy. An extensive description of the model can be found in Appendix A.

To account for the effects of the diurnal cycle and carbon partitioning, functional biomass and intracellular carbohydrate reserves were regarded as separate compounds. The carbohydrate reserves are referred to as 'sugar' in this study. Consequently, for each strain, two production rates were distinguished: the production of functional biomass (X') and of sugar (S).

Refer to Fig. 1 for an overview of the model structure. The overall microalgae production model consists of three modules: Location, time, and wavelength dependent light distribution (Module 1); specific light absorption, and photosynthetic sugar production (Module 2); partitioning of sugar towards biomass, and a sugar reserve pool (Module 3). The first module describes the location-specific light intensity and the light distribution in the culture during the day. These are based on solar elevations, Snell's law, Fresnel's equations, and Lambert-Beer's law, while neglecting the effect of light scattering. The second module describes the sugar production as a function of specific light absorption and, consequently, depends on the local light intensity, biomass concentration, and strain-specific characteristics. The third module represents the allocation of photosynthetically produced sugar to maintenance related processes, to the accumulation of carbohydrate reserves, and to the production of functional biomass. In addition, the partitioning of sugar is differentiated between the day and night periods during the diurnal cycle.

2.2. Strategy and assumptions

Two ordinary differential equations (Eqs. (A9) and (A10)) describe the change in production and respiration of the functional biomass and the sugar for each strain separately. The Matlab built-in solver for stiff differential equations (ode23s) based on the 2nd/3rd order Runge-Kutta method was used to numerically integrate the change in concentrations over the cultivation time. This results in the respective functional biomass and sugar concentrations as a function of time.

The simulated cultivation time was 100 days. We simulated both a Mediterranean location (Tunisia, Lat. 36.867°) with a high irradiance and clear sky and a temperate location (the Netherlands, Lat. 52.117°) with considerable cloud cover. One specific summer day (July 15th, day 196 of the year) was continuously repeated in the model for each location. All simulations began at 8:00 am local solar time. During the day, the dilution rate was maintained constant while there was no culture dilution during the night. The dilution rate was optimized for each strain and each location (Netherlands and Tunisia) to maximize the productivity (See Appendix D for optimization procedure). The optimal dilution rate was subsequently applied during the final simulations.

Theoretical antenna size mutants of *Chlorella sorokiniana* were simulated. The strain-specific characteristics $\left(\mu_m, m_S, Y_{X'/S}, q_S^{max}, x_{S,min}\right)$ of the mutants were kept identical to the experimentally determined characteristics of the wild type (Table A3 of Appendix E), i.e., only the biomass specific absorption cross section for each wavelength $\left(a_{X',\lambda}\right)$ was altered by multiplying $a_{X',\lambda}$ with 0.1-0.9, depending on the degree of antenna size reduction (90-10%). Throughout the entire day/night cycle, $a_{X',\lambda}$ was assumed to be constant. The wild type absorption cross section was measured under mass culture conditions with an incident light intensity of 1500 $\mu mol_{ph}\, m^{-2} s^{-1}$ and an outgoing light intensity of 10 $\mu mol_{ph}\, m^{-2} s^{-1}$. The antenna size mutation is assumed to be stable and not affecting any other cellular property, and the considered strains are assumed as not being sensitive to photoinhibition under the simulated light conditions. Different wild type contamination levels were considered as well as the scenario of a reverse mutation which was assumed to result in a contamination of one cell per cubic meter at the initiation of the 100-days simulation. One cell of *C. sorokiniana* corresponds to a mass of $1.4 \cdot 10^{-11}$ g, or 0.14 pg (Rosenberg et al., 2014). A reflective (80%) ground cover was simulated to be situated at the bottom of the photobioreactor pond to allow a fairer comparison of mutant and wild type performance.

The areal biomass productivity (r_{Cx}) was calculated by multiplying the total biomass concentration ($X' + S$) with the dilution rate (D) and the reactor depth (d_R):

$$r_{Cx} = (X' + S) \cdot D \cdot d_R \quad (1)$$

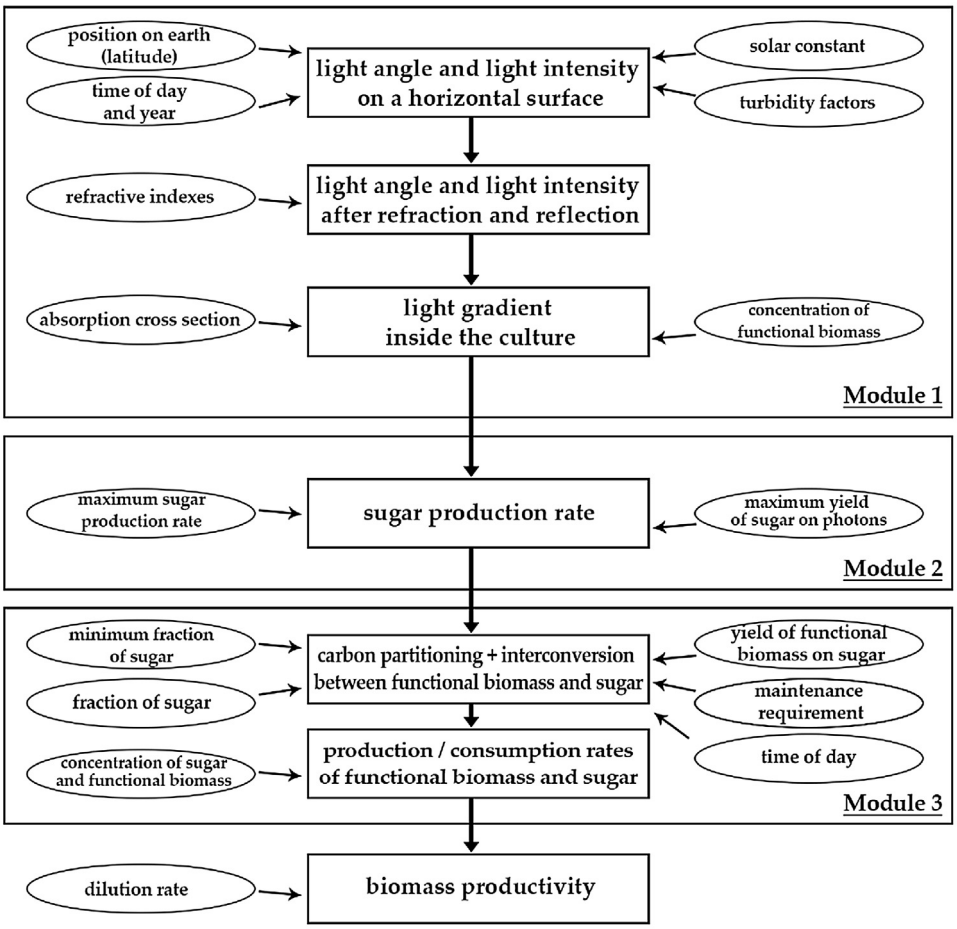

Fig. 1. Calculation scheme for the three modules. Module 1: location, time, and wavelength of specific light distribution; Module 2: photosynthetic sugar production; Module 3: sugar allocation towards biomass, the sugar reserve pool, and maintenance during the diurnal cycle. Model inputs are in ovals and calculated values in solid boxes.

3. Results

Simulations with the model were performed for monocultures of the wild type of *Chlorella sorokiniana* and for monocultures of the antenna size mutants with a varying absorption cross section $\left(a_{X',\lambda}\right)$ in the range of a 10–90% reduction compared to the wild type. In addition, monocultures of the antenna size mutants were 'contaminated' with wild type cells at various contamination levels in order to investigate the competiveness of the mutants and the dynamics of outcompetition. The wild type and the mutants were compared regarding their areal biomass productivity at two locations, the Netherlands and Tunisia, during a hypothetical summer season of 100 days. Refer to Appendix C for the light pattern of one summer day for both locations that was employed in all simulated days to obtain repetitive light conditions. For contaminated cultures, the loss of productivity as a result of the contamination with the wild type was also investigated.

3.1. Simulation overview

In Fig. 2A, the day/night cycle of one cultivation is illustrated for both the wild type and a mutant with an 80% antenna size reduction in Tunisia. The net sugar production rate ($X' \cdot (q_S - m_S)$) is a measure for the photosynthetic activity of the mutant culture. It is illustrated that the net sugar production rate of the mutant culture is considerably higher than that of the wild type culture only during the brightest hours of the day. In the night the sugar production rate is negative because sugar is used to build new functional biomass and sugar is partly respired to support both the growth processes as well as the maintenance related processes. The mutant culture exhibits greater losses of photosynthetically derived sugar during the night because of the higher biomass concentration and the associated maintenance requirements that must be satisfied. Please note that the functional biomass specific maintenance rate (m_s) is assumed to be the same for wild type and mutant. Therefore, the difference in sugar consumption rate between wild type and mutant is caused by the difference in biomass concentration.

Exemplary, the first 50 days of the 100 days cultivation period are shown for the mutant with an 80% antenna size reduction in Tunisia (Fig. 2B–D). As demonstrated later, a monoculture of this mutant results in the highest areal biomass productivity (r_{Cx}). It can be observed in greater detail on day 50 in Fig. 2B and C that, during the day, biomass is produced and the biomass concentration is increasing. However, in the morning and from 16:00 solar time onwards, the biomass concentration is decreasing as the result of the low incident light intensity in combination with culture dilution. The course of the cultivation is illustrated for monocultures of the mutant with and without contamination by the wild type. The shown contamination level is one wild type cell per cubic meter at day 0. The contamination has substantial effects on the course of the cultivation after approximately 27 days (Fig. 2B). The mutant concentration then decreases rapidly while the wild type concentration increases, which considerably reduces the biomass productivity. The wild type reaches a lower biomass concentration and lower productivity than the mutant. These effects are a result of the wild type absorbing more light per cell which leads to more

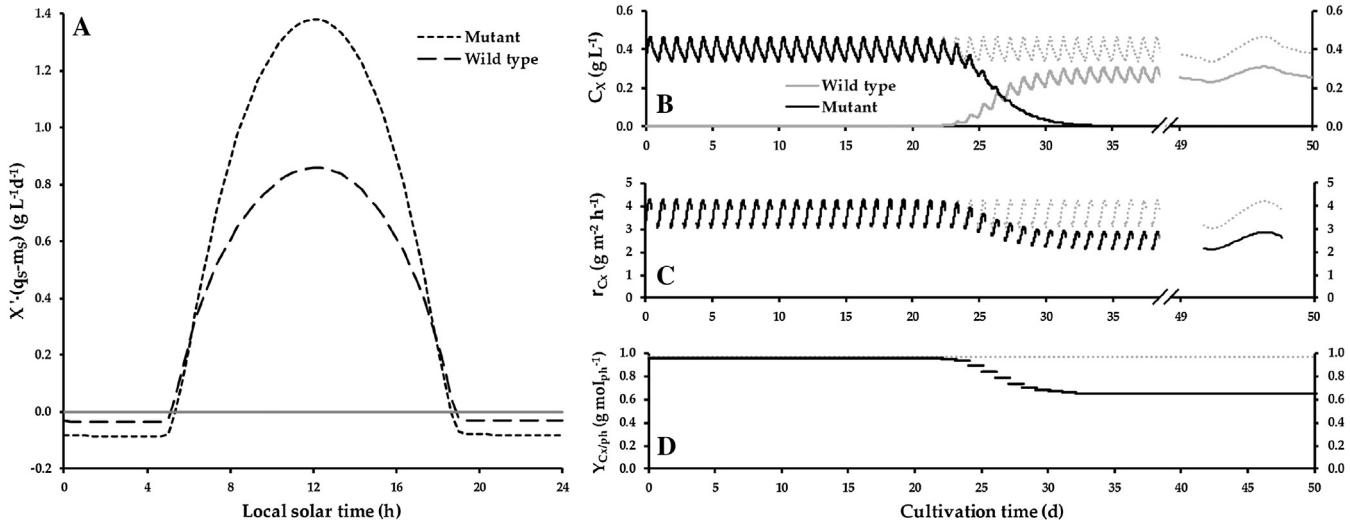

Fig. 2. (A) Net sugar production rate ($X'\cdot(q_S\text{-}m_S)$), a measure for the photosynthetic activity minus the maintenance, presented for the duration of one day/night cycle. In B, C, and D, an overview is provided of the first 50 d of a 100 d simulation of an antenna size mutant with 80% reduction in the absorption cross section ($a_{X',\lambda}$) in Tunisia. Day 50 is plotted on a different scale in B and C to illustrate the variation over the course of one day in greater detail. The culture is contaminated at t = 0 with one wild type cell per cubic meter. The dashed grey lines depict the scenario of an axenic mutant culture without contamination. (B) The biomass concentration (C_X) of the mutant and the wild type. (C) The daily areal biomass productivity (r_{Cx}) of the mixed culture as the sum of the productivity of mutant and wild type is depicted by the solid black line. (D) The biomass yield on incident light ($Y_{Cx/ph}$) averaged over one day is shown by the solid black line and is based on the mixed culture of wild type and mutant cells. The dilution rate was kept constant during the light period, and no dilution was applied during the night.

oversaturation and light loss. This is also manifested as a decrease of the biomass yield on light (Fig. 2D).

3.2. Monocultures of antenna size mutants and their wild type

The areal biomass productivity of antenna size mutants in a simulated outdoor raceway pond photobioreactor was investigated. The reduction in absorption cross section was normalized to the wild type, and a reduction of 10 to 90% was simulated. The areal biomass productivity of the mutant monocultures was found to increase with increasing antenna size reduction until a maximum is reached (Fig. 3A). The maximum productivities were found for cultures with antenna size reductions of 80% ($53.2\,g\,m^{-2}d^{-1}$) in Tunisia and 60% ($31.5\,g\,m^{-2}d^{-1}$) in the Netherlands. After the maximum, the biomass productivity decreases when the antenna size is further reduced.

Comparing the two locations, the areal biomass productivity was higher in Tunisia than in the Netherlands for all of the mutants and the wild type. Because of the higher irradiance, both the biomass concentrations and the optimal dilution rates were higher in Tunisia than in the Netherlands. In Tunisia, the increase of the productivity with the antenna size reduction is steeper and leading to a sharper maximum than in the Netherlands. A relative productivity increase of 39% in Tunisia and of 16% in the Netherlands was observed for the best performing mutant strain.

The loss in productivity after the maximum has been reached is primarily caused by the fact that light, after being reflected at the bottom due to the ground cover (i.e. liner), is leaving the photobioreactor pond unused at the surface when applying a very high antenna size reduction. It is important to note that a white liner was simulated with an 80% reflectivity as described in Appendix B. For an antenna reduction of 90% in Tunisia, up to $100\,\mu mol_{ph}\,m^{-2}s^{-1}$ is lost in this way at solar noon. In addition, the higher costs for maintenance required for the high biomass concentration further decrease the productivity. The maintenance requirement is assumed to be a constant and equal for all mutants and the wild type. Consequently, the relative maintenance costs increase up to 24% in the Netherlands for a 90% $a_{X'}$ reduction (See Fig. 3A). At moderate antenna size reductions only 10% of the total produced sugar is consumed for the purpose of maintenance. This means that at high antenna size reduction a rapidly increasing fraction of photosynthetically produced sugar is used for maintenance instead of being incorporated into new biomass. The effect of maintenance is higher for lower irradiance conditions as present in the Netherlands.

The relation between antenna size reduction and photosynthetic efficiency under saturating light conditions is also reflected in the biomass yield on light (Fig. 3B). Because of the higher irradiance in Tunisia, overall yields are lower than in the Netherlands. Only beyond 80% antenna size reduction the biomass yield on light was higher in Tunisia than in the Netherlands. For small antennae, light oversaturation in Tunisia is relatively low while the light levels during the majority of the day are above $1000\,\mu mol_{ph}\,m^{-2}s^{-1}$ and even reach $1800\,\mu mol_{ph}\,m^{-2}s^{-1}$ at solar noon (See Appendix C).

3.3. Culture dynamics after mutant monoculture contamination by wild type cells

Antenna size mutant monocultures with a varying reduction in absorption cross section $\left(a_{X',\lambda}\right)$ were simulated as being contaminated with different levels of wild type cells. In this way the rate at which mutant cultures are overgrown was investigated as a function of the contamination level and antenna size reduction. Fig. 4A illustrates the effect of different contamination levels on the time it takes for wild type cells to become the dominant strain in the culture. Only the results for Tunisia are shown. The optimal antenna size reduction for Tunisia, 80%, was selected in order to study the effect of the contamination level. At the highest contamination level of 1%, the decrease in mutant biomass concentrations becomes apparent already after three days. Lower contamination levels extend the duration that the antenna size mutant is the dominant strain and during this period light is used at a higher efficiency compared to the situation in which the wild type is the dominant strain. However, even in the best case scenario that was considered, with a contamination of only one cell per cubic meter,

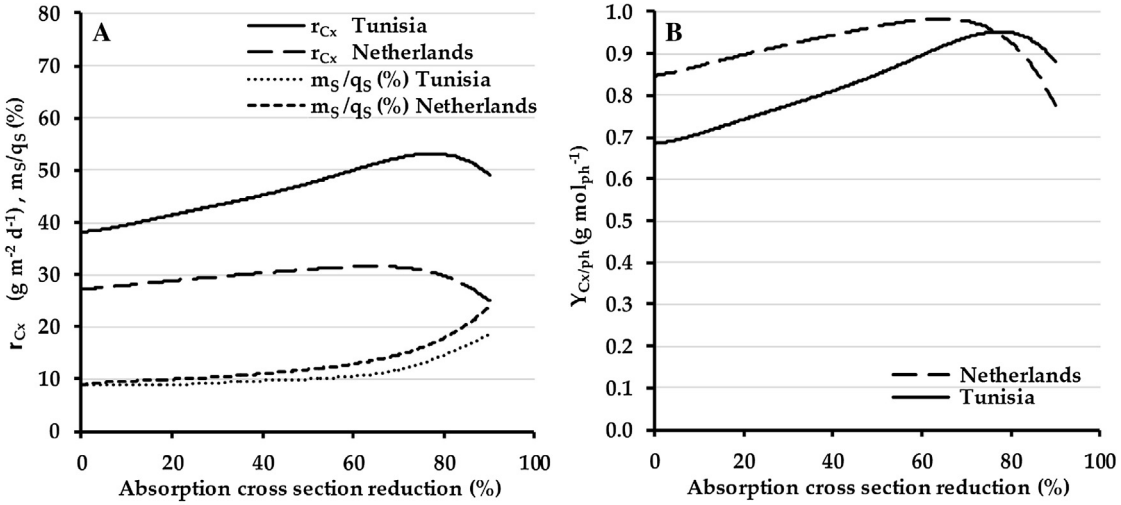

Fig. 3. (A) Biomass productivity (r_{Cx}) and relative costs of maintenance processes (m_S/q_S,%), i.e the fraction of produced sugar used for maintenance and not for growth. (B) biomass yield on incident light ($Y_{Cx/ph}$) presented for the wild type (0% reduction) and antenna size mutant cultures. For the calculation of the biomass yield on light, the daily averaged productivity is normalized to the daily amount of incident light on the photobioreactor.

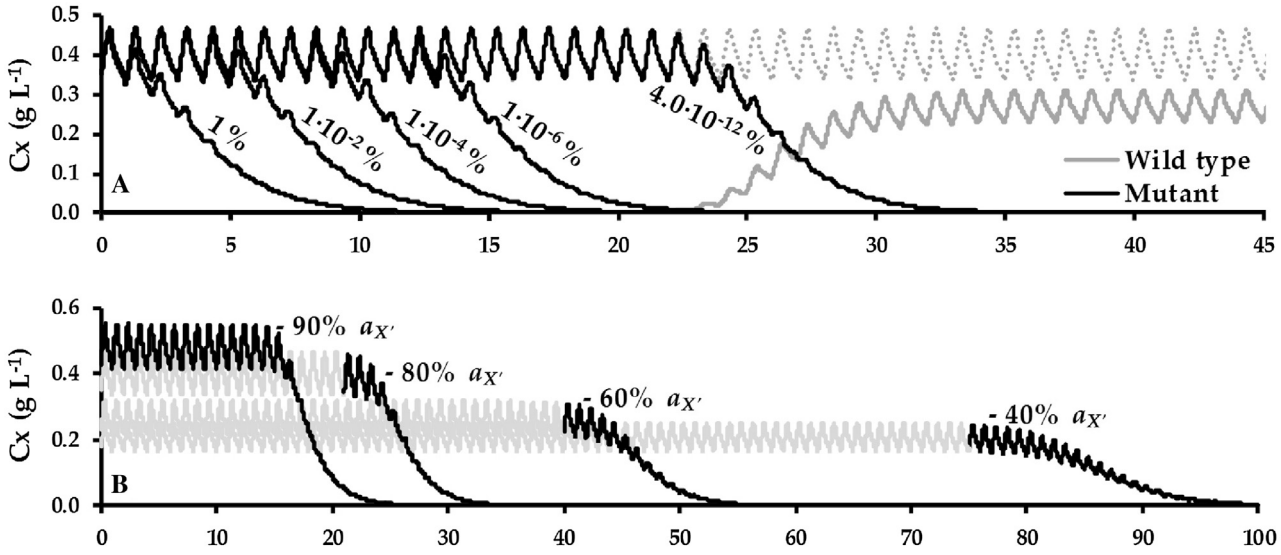

Fig. 4. (A) Effect of the contamination level on the rate at which antenna size mutants are overgrown by wild type cells in a simulated raceway pond photobioreactor with a depth of 0.2 m, situated in Tunisia. The mutant monocultures have an 80% reduction in the absorption cross section ($a_{X'}$). The dashed line indicates the scenario of a mutant monoculture with no contamination. Only for the lowest contamination level ($4.0{\cdot}10^{-12}$%, or 1 cell m^{-3} at day 0) the associated increase in wild type biomass concentration is illustrated by the solid grey line. (B) Effect of antenna size reduction on the rate at which the mutant monocultures are overgrown by the wild type cells. For clarity reasons, the wild type concentration is not presented. The contamination level for these simulations equal one wild type cell per cubic meter at day 0.

the mutants were overgrown before half of the simulated summer season (100 days) had passed.

In addition to the contamination level, the effect of the antenna size reduction was investigated (Fig. 4B). Again, one cell per cubic meter was chosen as the contamination level in a monoculture in Tunisia. Clearly, greater reductions in antenna size result in less competitive mutants and, therefore, the mutants with the highest potential in terms of mass culture productivity are most vulnerable and rapidly overgrown by wild type cells within one simulated summer season. For antenna size reductions below 40%, the mutants remain the dominant strain in the culture during the simulated season. However, as shown before in Fig. 3, a 40% reduced antenna size mutant does not exploit the full potential of antenna size reduction.

4. Discussion

In accordance with our expectations, the areal biomass productivity was higher in Tunisia than in the Netherlands for all mutants and the wild type. Up to a 39% increase in productivity was estimated for an 80% antenna size reduced mutant compared to the wild type. In contrast to Tunisia, in the Netherlands under the most optimistic conditions, only a 16% increase in productivity could be obtained compared to the wild type cultivation. These numbers emphasize that both a considerable antenna size reduction and high irradiance are required to obtain substantial gains in productivity. Most antenna size mutants that have been created do not exhibit such high antenna size reductions (de Mooij et al., 2014). In Tunisia, saturating light conditions are present over a longer period of the day than in the Netherlands. Therefore, any reduction in

absorption cross section reduces oversaturation and thus increases light use efficiency (Melis et al., 1998; Mussgnug et al., 2007b; Mitra and Melis, 2008; de Mooij et al., 2014; Zhu et al., 2010). The results show a clear potential for the use of antenna size mutants in high irradiance locations such as Tunisia.

The theoretical maximum biomass yield on light ($Y_{Cx/ph}$) for *Chlorella sorokiniana* with nitrate as nitrogen source is approximately 1.57 g mol_{ph}^{-1} (Kliphuis et al., 2010). Compared to this value, the simulated yields for wild type cultivation in the Netherlands (0.85 g mol_{ph}^{-1}) and Tunisia (0.68 g mol_{ph}^{-1}) show room for improvement. However, in large scale production, the theoretical maximum cannot be reached under saturating light. Using the optimal 80% antenna size reduction in Tunisia, the biomass yield on light energy was simulated to increase to 0.95 g mol_{ph}^{-1}, which is high for large scale cultivation in an environment of high irradiance. The estimated productivities and biomass yields on light are in the expected ranges based on empirical data of *C. sorokiniana* (Zijffers et al., 2010), which supports the reliability of the presented results.

Smaller antenna sizes increase the productivity in environments of high irradiance. However, there is an upper limit because the higher the antenna size reduction is, the higher the optimal biomass concentration that is required to absorb the incident light intensity. At higher antenna size reductions, it becomes practically impossible to harvest all of the light that is available around solar noon. Consequently, especially green light is leaving the photobioreactor unused after being reflected at the bottom. In addition, 20% of the light that reaches the pond floor is absorbed by the pond liner which means that a more 'transparent' culture will also result in more loss of light at the bottom. Theoretically, the problem could be alleviated by adjusting the biomass concentration over the course of the entire day, however, in practice, it is impossible to maintain an optimal biomass concentration throughout the entire day as biomass growth is too slow to respond to sunrise, sunset and the fluctuation light conditions during the day (Pruvost et al., 2015).

As the maintenance requirement per cell is assumed to be constant, the total energy spent on maintenance increases linearly with the biomass concentration. In the range of 10–80% antenna size reduction, the increase in maintenance costs is not a big issue since the concomitant increase of the productivity is higher, and this outweighs the maintenance losses. However, as depicted in Fig. 3A, the fraction of sugars utilized for maintenance can be as high as 24% for a 90% antenna size reduction in the Netherlands. Therefore, an optimal antenna size reduction was identified based on the model. In addition to this energetically optimal antenna reduction, in practice, antenna size reduction may possibly be limited by structural constraints as there appears to be a minimum amount of chlorophyll molecules that is required for the assembly of the photosystem core complexes (Glick and Melis, 1988).

A reflective ground cover (i.e., liner) was simulated to be situated at the bottom of the photobioreactor pond to allow a fairer comparison of mutant and wild type performance. Without light reflection at the bottom, even a higher fraction of the incident light intensity would be lost (absorbed at the pond floor) in the mutant culture in comparison to the wild type culture. At high antenna size reductions, the reflective liner could not prevent considerable light losses in mutant monocultures as unabsorbed light was reflected on the pond floor but subsequently could not be fully absorbed in the suspension after which it left the raceway pond reactor at the liquid surface.

The choice for infinite width and length of the theoretical photobioreactor has the consequence that shadow formation by walls and reactor equipment can be neglected. The model therefore overpredicts the productivity compared to real systems. This effect will decrease with the increasing reactor size, as the walls and equipment are relatively small in large reactors. The assumption of constant depth means that precipitation and evaporation are neglected, or supposed to balance each other. The effect of a changing depth, and therefore a changing biomass concentration, could be easily implemented but similar to using real weather data, it would blur the focus on the effect of antenna size reduction.

Cells in a mixed culture of wild type and antenna size mutants are competing for light energy. Cells with a higher pigmentation have a competitive advantage in this situation, as has recently been verified in competition experiments with phycobilisome-deficient cyanobacteria and the corresponding wild type (Agostoni et al., 2016). However, at the high light exposed volume fraction of the reactor, the most competitive cells, with the highest absorption cross section, are more oversaturated with light energy, resulting in heat dissipation. Stated differently, competitiveness comes at a cost of light use efficiency and productivity. Antenna size mutants grow slower than the wild type in the light limiting part of the reactor which makes them less competitive. The lower competiveness as well as the higher light use efficiency of the mutants were confirmed in our simulations. As the photobioreactor productivity of a mutant culture eventually returns to the level of the wild type productivity after a contamination, it can be concluded that the biggest increase in productivity obtained with antenna size reduction also results in the most significant losses upon contamination.

The lower the antenna size reduction, the more competitive the organism becomes and the longer it takes before it is outcompeted by the wild type. Contamination can be caused by wild type cells physically entering the photobioreactor or by mutant cells losing their phenotype after a reverse mutation, after which the natural pigment content is restored. In regard to the contamination level, it became evident that, even in the most optimistic scenario with a minimal contamination of one cell per cubic meter, the effects of contamination are considerable. Moreover, the contamination level is unpredictable and could be higher than the assumed one cell per m^3. Therefore it can be stated that, unless novel methods are discovered to increase the competitive power of antenna size mutants, the consequences of wild type contamination severely threaten the potential application of antenna size mutants in large-scale long-term production processes.

We have demonstrated that even a contamination level as low as one cell per cubic meter at the beginning of cultivation can substantially reduce the potential productivity increase that was aimed for by using antenna size mutants. Once a contamination has been detected, thorough cleaning and disinfection of the photobioreactor pond is required with no tolerance for remaining wild type cells or other photosynthetic organisms. This is time consuming and expensive and will probably outbalance the cost reduction that could have been obtained by the application of antenna size reduction.

Would it be possible to increase the competitive power of antenna size mutants? In the study of Flynn et al., the mutants were assumed to have additional properties that made them more competitive. They simulated mutants with an increased growth rate and nutrient use efficiency, a decreased minimum phosphorous and nitrogen quota, a lower maintenance requirement and, under these conditions, the mutant was expected to outcompete the wild type (Flynn et al., 2013). It remains doubtful, however, whether a mutant with all of the aforementioned properties can be designed in practice and remain stable regarding all mutations. For example, in order to obtain a higher biomass specific growth rate, many enzymatic steps must be performed at a higher rate which does not appear to be feasible. Another method to improve the competitiveness of the mutant rather than changing its growth characteristics is the application of extreme conditions. This condition should ideally affect the viability of the wild type strain but not that of the mutant. One could think of a built-in resistance of the mutant, for example, tolerance to low/high temperatures or a tolerance to

high salt concentrations. However, this would still create a selective environment that rewards invasive species that actually have such a capability (Mooij et al., 2015). Smart techniques are required to enforce the elimination of the wild type while maintaining the mutant cells. Perhaps the wild type's higher sensitivity to light can be exploited as this makes them more prone to photoinhibition while antenna size mutants would only experience photoinhibition at much higher light intensities. Wild type cells possibly have to spend more energy on photosystem II repair processes than antenna size mutants because their higher light absorbance rate will also increase the irreversible damage to the photosystems. To win the competition, the specific growth rate of the mutant should be higher than that of the wild type. At solar noon in Tunisia, the biomass specific growth rate of an 80% reduced mutant is 1.4 d^{-1} versus 2.2 d^{-1} for the wild type according to our growth model. Consequently, severe chronic photoinhibition would be required for the wild type to shift the equilibrium towards the mutant. For *Chlorella sorokiniana* such severe photoinhibition has not been observed up to light levels of 2000 $\mu mol_{ph}\ m^{-2}s^{-1}$ (Cuaresma et al., 2011; Franco et al., 2012) and for this reason photoinhibition was not included in this model.

A more complex dynamic model was presented by Flynn et al. (Flynn et al., 2013, 2010; Flynn, 2001). In accordance with our findings, Flynn and coworkers estimated that under continuous light (1000 $\mu mol_{ph}\ m^{-2}s^{-1}$), the use of antenna size mutants will lead to an increased biomass productivity, and the mutants will be outcompeted by the wild type after a contamination (Flynn et al., 2010). The strength of our model is its simplicity and the fact that we only considered mutants with a reduction of the absorption cross section without additional traits. The repetitive light pattern and the lack of seasonal light and temperature variability has the advantage that effects can be unequivocally assigned to the antenna size reduction or the contamination level which was the purpose of this study. The estimations of our model provide a realistic view of the potential of antenna size mutants under large scale outdoor conditions. The productivity of our mutants was limited by the inevitable steep light gradient in mass cultures, the low light absorption capacity of mutants, and the fact that the total maintenance requirement can become a critical factor at substantial antenna size reductions. We also included the impact of day/night cycles on microalgal growth. Even though the model includes several simplifications such as that photoinhibition was not included, it is capable of predicting important trends which can be used as input for future research.

5. Conclusions

A theoretical model was presented to simulate cultivations of antenna size mutants and the competition with their wild type under mass culture conditions. As was expected, the comparison of Tunisia with the Netherlands demonstrated that a substantial increase of productivity is only possible in a location of high irradiance. In addition, a considerable antenna size reduction (80%) is required to achieve maximal culture productivity. Mutants with such an antenna size reduction have not been obtained yet in practice. At very high antenna size reduction, it becomes difficult to efficiently absorb all incident light because of the low absorption capacity. In addition, high biomass concentrations are required to absorb all light, which increases cellular maintenances costs. The higher the antenna reduction is, the more sensitive the cultivation process becomes for competition with a full antenna strain. According to the model, antenna size mutants will always lose the competition for light with their wild type and the rate of outcompetition was ascertained to increase with decreasing antenna size and with increasing contamination levels. Based on these findings it can be concluded that the competitiveness of the mutants strains is an important factor that determines whether long-term stable cultivation can be achieved in mass cultures.

Acknowledgements

This work is part of the research programme of the Foundation for Fundamental Research on Matter (FOM) which is part of the Netherlands Organization for Scientific Research (NWO). This project (10TBSC12-3) was conducted within the research programme of BioSolar Cells, co-financed by the Dutch Ministry of Economic Affairs.

Appendix A. : Microalgae growth model

(A1) Module 1: Light distribution in a photobioreactor

In this algae production model, a hypothetical photobioreactor is studied (Fig. A1) that represents a pond with a constant depth (d_R, 0.20 m) and with infinite width and length. The only interface that is considered for reflection and refraction is the air-water interface since the culture is directly in contact with the air at the culture surface. The light intensity on the culture surface must be determined to later predict the light distribution within the culture.

The light intensity gradient in the microalgae culture is calculated in three consecutive steps. First, the light intensity on a horizontal surface on earth is calculated neglecting the effect of atmospheric light absorption (Velds et al., 1992). Second, the absorption of the atmosphere due to its turbidity is incorporated (Velds et al., 1992). In the third step, the refraction and reflection of light passing the air water interphase (Cooper, 1969; Kasten and Czeplak, 1980; Goldstein, 2010) is included to obtain the intensity and directionality of this light that enters the microalgae culture ($I_{ph,0}$). For an extensive description of the equations used to calculate the incident light intensity, refer to Appendix C.

The incident light intensity on a horizontal surface ($I_{ph,0}$) is used as an input in Eq. (A1), which is based on Lambert-Beer's law.

$$I_{ph,\lambda,down}(z) = I_{ph,0} \cdot E_{n,\lambda} \cdot e^{-\left(a_{X',\lambda_{WT}} \cdot X'_{WT} + a_{X',\lambda_{MU}} \cdot X'_{MU}\right) \cdot z \cdot \frac{1}{\cos\theta'_z}} \quad \text{(A1)}$$

$E_{n,\lambda}$ (nm^{-1}) represents the relative sunlight distribution for the range of photosynthetic active radiation (see Appendix E for values). The absorption cross sections of the wild type strain and the mutant are denoted by $a_{X',\lambda_{WT}}$ and $a_{X',\lambda_{MU}}$, respectively. In Eq. (A1), z is the position in the pond along the vertical path equaling zero at the reactor surface and 'd_R' at the bottom of the reactor. The length of the light path in the culture is influenced by the angle between the refracted sunrays and the perpendicular to the culture surface (angle θ_z', Fig. A1). In the model, the position z is multiplied with the enhancing factor, the inverse of the cosine of θ_z', to correct for the lengthening of the optical path at increasing θ_z'. An increasing optical path increases the chance of light absorption and results in a steeper light gradient in the z-direction.

To minimize light losses at the bottom of the pond and to obtain a fairer comparison between wild type and mutant culture productivity, the pond floor was simulated to be covered with a white reflective ground cover. This cover diffusively reflects 80% (Meinhold et al., 2010) of the light at the bottom back into the culture. Moreover, the application of white liners is also common practice in the raceway pond construction. The addition of a reflective liner results in a second light flux $I_{ph,\lambda,up}(z)$ from the pond floor back to the culture surface. The light intensity in the culture only resulting from this flux is described by:

$$I_{ph,\lambda,up}(z) = I_{ph,\lambda,down}(d_R) \cdot f_R \cdot e^{-\left(a_{X',\lambda_{WT}} \cdot X'_{WT} + a_{X',\lambda_{MU}} \cdot X'_{MU}\right) \cdot (d_R - z) \cdot \frac{1}{\cos\theta'_{z,dif}}} \quad \text{(A2)}$$

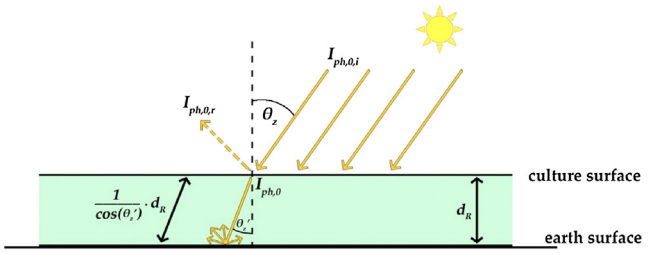

Fig. A1. Schematic overview of the raceway pond photobioreactor. The sunlight hits the culture surface with the light intensity $I_{ph,0,i}$ at the zenith angle θ_z. The light is partly reflected $\left(I_{ph,0,r}\right)$ and partly transmitted into the culture $\left(I_{ph,0}\right)$. The refraction at the culture surface leads to the refracted zenith angle θ_z'. The light reaching the bottom of the pond is, in part (80%), diffusively reflected back into the culture by a white ground cover.

with d_R being the reactor depth and f_R being the fraction of reflected light. The inverse of the cosine of $\theta_{z,dif}{}'$ is the factor with which the reflected optical light path is extended. The diffuse reflection corresponds to an average angle $\theta_{z,dif}{}'$ of 60°.

(A3) Module 2: Photosynthetic sugar production

To model the competition for light in a culture of an antenna size mutant contaminated with its wild type, the specific light absorption rates of both strains must be distinguished. The specific light absorption rates then allow the calculation of specific sugar production rates for each strain. The sugar production rate $\left(q_{S_i}\right)$ of one organism (indicated by index i) in a culture containing wild type and mutant cells can be described according to the hyperbolic tangent model of Jassby and Platt (Jassby and Platt, 1976):

$$q_{S_i} = q_S^{max} \cdot tanh\left(\frac{q_{ph,i} \cdot Y_{S/ph,m}}{q_S^{max}}\right) \tag{A3}$$

The calculation of the sugar production rate is based on the photon absorption rate $\left(q_{ph,i}\right)$, the maximum yield of sugar on photons $\left(Y_{S/ph,m}\right)$, and the maximum sugar production rate $\left(q_S^{max}\right)$, (see Table A3 of Appendix E for values). The biomass specific light absorption rate $\left(q_{ph,\lambda,i}\right)$ can be described for wild type $(i = WT)$ and mutant $(i = MU)$ in one photobioreactor simultaneously by utilizing Lambert-Beer's law:

$$\frac{dI_{ph,\lambda,down}}{dz} = I_{ph,\lambda,down}(z) \cdot \left(a_{X'_{WT},\lambda} \cdot X'_{WT} + a_{X'_{MU},\lambda} \cdot X'_{MU}\right) \cdot \frac{1}{\cos\theta'_z} \tag{A4}$$

$$\frac{dI_{ph,\lambda,up}}{dz} = I_{ph,\lambda,up}(z) \cdot \left(a_{X'_{WT},\lambda} \cdot X'_{WT} + a_{X'_{MU},\lambda} \cdot X'_{MU}\right) \cdot \frac{1}{\cos\theta'_{z,diff}} \tag{A5}$$

$$q_{ph,\lambda,i} = \left(-\frac{dI_{ph,\lambda,down}}{dz} + \frac{dI_{ph,\lambda,up}}{dz}\right) \cdot \frac{1}{X'_i} \cdot \frac{a_{X'_i} \cdot X'_i}{a_{X'_{WT},\lambda} \cdot X'_{WT} + a_{X'_{MU},\lambda} \cdot X'_{MU}} \tag{A6}$$

with the light gradients $\frac{dI_{ph,\lambda,down}}{dz}$ and $\frac{dI_{ph,\lambda,up}}{dz}$, the concentration of functional biomass (X'_i), the absorption cross section $\left(a_{X'_i,\lambda}\right)$, the local light intensity $\left(I_{ph,\lambda}(z)\right)$, and the factor $\left(\frac{1}{\cos\theta'_z}\right)$ that corrects the light path for its deviation from the z direction. Apparently, the light regime in the reactor (Eqs. (A4) and (A5)) is dictated by the total light absorption capacity of both the wild type and mutant strain. The biomass specific light absorption rates $(q_{ph,\lambda,i})$(Eq. (A6)) depend on the absorbed fraction of this total light energy which is based on the light absorption capacity and biomass concentration of each strain. Eqs. (A4)–(A6) are combined to give:

$$q_{ph,i,\lambda}(z) = a_{X',\lambda_i} \cdot \left(I_{ph,\lambda,down}(z) \cdot \frac{1}{\cos\theta'_z} + I_{ph,\lambda,up}(z) \cdot \frac{1}{\cos\theta_{z,diff'}}\right) \tag{A7}$$

By combining Eqs. (A3) and (A7) and adding the wavelength dependency of $Y_{S/ph,m}$, the specific sugar production rates of the mutant and wild type were obtained:

$$q_{S_i}(z) = q_S^{max} \cdot tanh\left(\frac{\sum_{\lambda=400}^{\lambda=700}(q_{ph,i,\lambda}(z) \cdot Y_{S/ph,m,\lambda}) \cdot \Delta\lambda}{q_S^{max}}\right) \tag{A8}$$

The specific sugar production rates (Eq. (A8)) were concurrently simulated in one photobioreactor for both strains to model the competition for light. The produced sugar is partly used for maintenance related processes, partly stored in the sugar reserve pool, and partly used for production of new functional biomass.

(A9) Module 3: Partitioning of produced sugar during the diurnal cycle

The carbohydrate starch is an important energy reserve for the growth of microalgae in day/night cycles (Sharkey, 2015; Ogbonna and Tanaka, 1996). Synthetized starch is stored as semi-crystalline granules (Sonnewald and Kossmann, 2013) and can be oxidized by the cell to gain energy and reduce carbon upon demand (Lacour et al., 2012). The accumulation of starch occurs during the day when it serves as an energy sink while the degradation primarily occurs during the night to provide energy and carbon (Lacour et al., 2012; Sukenik and Carmeli, 1990; Post et al., 1985; Fábregas et al., 2002).

A mechanism of carbon partitioning during the diurnal cycle was developed. This mechanism includes partitioning of the photosynthetically produced sugar to the functional biomass and the sugar reserve pool. The longer the night period and the lower the current sugar reserves, the more sugar is stored in the sugar pool during the day to accumulate sufficient reserves for the entire night period. Additionally, sugar from the sugar pool is converted into functional biomass at a rate that depends on the sugar availability. The conversion rate will automatically be re-adjusted in such a way that it would be stable until the end of the night if no additional sugar is generated. This leads to a minimum sugar fraction in the total biomass at the end of the night.

The production rates of functional biomass and sugar are described in two differential equations (Eqs. (A9) and (A10)) which are applied on both strains simultaneously:

$$\frac{dX'_i}{dt} = \underbrace{q_{S,i} \cdot \left(1 - \left(\frac{x_{S,min,i}}{x_{S,i}}\right)^{\frac{P_{light}}{24}}\right) \cdot X'_i}_{\text{term 1: accumulation by photosynthesis}} - \underbrace{m_{X'} \cdot X'_i}_{\text{term 2: maintenance}} + \underbrace{\frac{x_{S,i} - x_{S,min,i}}{t_{end\ of\ night} - t} \cdot Cx_i \cdot Y_{X'/S}}_{\text{term 3: conversion of S into X'}} - \underbrace{D(t) \cdot X'_i}_{\text{term 4: dilution}} \tag{A9}$$

$$\frac{dS_i}{dt} = \underbrace{q_{S,i} \cdot \left(\frac{x_{S,min,i}}{x_{S,i}}\right)^{\frac{P_{light}}{24}} \cdot X'_i}_{\text{term 1: accumulation by photosynthesis}} - \underbrace{m_S \cdot X'_i}_{\text{term 2: maintenance}} - \underbrace{\frac{x_{S,i} - x_{S,min,i}}{t_{end\ of\ night} - t} \cdot Cx_i}_{\text{term 3: conversion of S into X'}} - \underbrace{D(t) \cdot S_i}_{\text{term 4: dilution}} \tag{A10}$$

With:

$m_{X'} = 0$ for $x_{S,i} > x_{S,min,i}$

$m_S = 0$ for $x_{S,i} = x_{S,min,i}$

The biomass accumulation rate (Eq. (A9)) and the sugar accumulation rate (Eq. (A10)) depend, among others, on the total biomass concentration (Cx_i) and the concentration of functional biomass (X'_i) and sugar (S_i). $m_{X'}$ is the maintenance requirement $\left(mol_{X'} \cdot {mol_{X'}}^{-1} \cdot s^{-1}\right)$ covered by degradation of functional biomass. The molar fraction of sugar in biomass is given as $x_{S,i} = S_i/(X'_i + S_i)$. The index i indicates that the equations need to be separately applied on the two strains, wild type ($i = WT$) and mutant ($i = MU$). The cultivation time, t (0–24 h), is the local solar time.

The differential equations describing the accumulation of functional biomass and sugars in the photobioreactor (Eqs. (A9) and (A10)) both include four terms. The first term depends on the sugar production rate (Eqs. (A8)) and, therefore, the amount of absorbed light. Carbon fixated and reduced by photosynthesis partitions between the synthesis of functional biomass and the sugar pool. The partitioning depends on the sugar fraction of biomass $\left(x_{S,i}\right)$ at the investigated time point and the duration (hours) of the light period $\left(P_{light}\right)$ in one day/night cycle of 24 h. The shorter the light period, the more sugar reserves are needed during the night to cover the maintenance requirement and support the generation of functional biomass in the dark (Lacour et al., 2012). To restore the sugar reserves for the consumption during the night, low sugar fractions in the biomass lead to a high allocation rate of photosynthetically produced sugar to the sugar pool. This behavior is simulated by a Droop based equation (Gibson et al., 2008).

The second term of the equations Eqs. (A9) and (A10) describes the specific maintenance requirement of the functional biomass. The maintenance requirement (m_S) is primarily covered by the respiration of sugar. Sufficient sugar reserves to fulfill maintenance requirements are ensured by the sugar accumulation mechanism. However, in the exceptional case that the sugar reserves are too low ($x_{S,i} \leq x_{S,min,i}$), the only way to fulfill maintenance requirements ($m_{X'}$) is by the degradation of functional biomass, as shown by the second term of Eq. (A9).

Independent from light conditions, the third term ensures the conversion of sugar to functional biomass. This rate is linear during the night and results in the minimum sugar fraction $x_{S,min,i}$ at the end of the night. Based on starch turnover (Klein, 1987), a minimum production rate of functional biomass is ensured over the entire course of the day as soon as sugar has been accumulated. First, the released sugar is used for maintenance related processes, and the remaining sugar subsequently enters the functional biomass production. This way, functional biomass is produced during the night at the expense of the sugar pool. Sugar is employed for the production of functional biomass according to the functional biomass yield on sugar $Y_{X'/S}$. This yield has a value less than 1, reflecting the fact that a significant portion of the sugar needs to be respired to retrieve sufficient energy in the form of ATP to incorporate the remaining sugar into functional biomass.

The last term of the differential equations describes the removal of functional biomass and the sugar reserves by the applied system dilution, as the raceway pond reactor is operated as a chemostat. Dilution is only applied during daylight hours.

Appendix B. : Equations to calculate location and wavelength-specific light distribution

(A11) Solar power and sunlight angle on a horizontal surface

In this calculation, the effect of the turbidity of the atmosphere is first neglected, however, the predicted solar power is later corrected for the contribution of atmospheric absorption. The solar power on a horizontal surface (E_e) depends on the intensity of sunlight reaching the earth and the zenith angle $\left(\theta_z, \text{Eq.A12}\right)$. The latter is the angle between the sunrays and the perpendicular to the earth's surface (Fig. 3).

$$E_e = S_0 \cdot \frac{\bar{R}^2}{R^2} \cdot \cos\theta_z \approx S_0 \cdot \left(1 + 0.033 \cdot \cos\left(\frac{360}{365} \cdot (d-1)\right)\right) \cdot \cos\theta_z \quad \text{(A11)}$$

In Eq. (A11), all light is assumed to pass from the center of the sun to the earth neglecting effects of the atmosphere. The yearly averaged solar power on earth is described by the solar constant (S_0, $1367 \text{W} \cdot \text{m}^{-2}$ (Fröhlich and Brusa, 2016)). The solar power varies with the factor $\frac{\bar{R}^2}{R^2}$ over the year due to the ellipsoidal shape of the earth's orbit (Duffie and Beckman, 2016). The daytime and the location dependency of the insolation are both described by the zenith angle:

$$\theta_z = \cos^{-1}\left(\sin\phi \cdot \sin\delta + \cos\phi \cdot \cos\delta \cdot \cos\omega\right) \quad \text{(A12)}$$

The latitude (ϕ) is directly named in Eq. (A12) while the longitude is indirectly included through the hour angle ($\omega = 15 \cdot (t_{solar} - 12)[^\circ]$). The position of the sun is highest at 0° or $t_{solar} = 12\text{h}$. The tilt of the earth relative to the sun throughout the year is described by the solar declination $\left(\delta = 23.45 \cdot \sin\left(\frac{360 \cdot (284+d)}{365}\right)[^\circ]\right)$.

The solar power neglecting the atmosphere (E_e) can now be corrected for atmospheric absorption. As a simplification, the total global irradiation is considered as direct light even though it includes a diffuse part. Thus, the solar power reaching the earth at a specific location (G_{clear}) and with a clear sky is described as:

$$G_{clear} = 0.84 \cdot E_e \cdot e^{\left(-\frac{0.027 T_L}{\cos\theta_z}\right)} \quad \text{(A13)}$$

The turbidity factor of the atmosphere by Linke (T_L) has been determined experimentally. Under a clear sky, the factor only depends on the time during the year and the location on earth (Velds et al., 1992; Chaâbane et al., 2004). The calculated surface-specific solar power using the turbidity factor is converted into the light intensity. The light intensity in the range of the photosynthetic active radiation (PAR, 400 to 700 nm) is calculated using a conversion factor according to ASTM G173-03 Reference Spectra derived from SMARTS v. 2.9.2:

$$I_{ph,0,i} = G_{clear} \cdot 1.982 \cdot 10^{-6} \frac{\text{mol}_{\text{ph,PAR}}}{\text{J}_{\text{solar}}} \quad \text{(A14)}$$

(A15) Light gradient resulting from refraction and reflection on the culture surface

The sunlight with the intensity $I_{ph,0,i}$ hits the culture surface which is assumed to have the same properties as a water surface. Two effects occur there simultaneously; light is refracted and reflected. Due to refraction, the zenith angle $\left(\theta_z\right)$ changes according to Snell's law to θ_z'. Thus, the factor $\left(\frac{1}{\cos(\theta_z')}\right)$ describing the light path dependent on the culture depth reads as:

$$\frac{1}{\cos\left(\theta_z'\right)} = \frac{1}{\cos\left(\sin^{-1}\left(\frac{n_{air}}{n_{water}} \cdot \sin\theta_z\right)\right)} \quad \text{(A15)}$$

The enhancing factor (Eq. (A15)) is based on the refractive indexes of air (n_{air}) and water (n_{water}) and trigonometric equations. This expression is used to relate the culture depth to the light path. By applying Lambert-Beer's, this affords calculation of the light distribution inside the culture. The incident light intensity is reduced compared to the description in Eq. (A14) since light is partly reflected by the culture surface and partly transmitted into the culture. The reflected light intensity is subtracted from

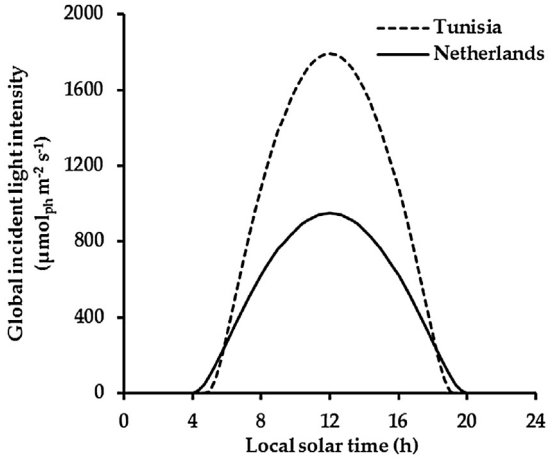

Fig. A2. Global incident light intensity in the PAR range on a horizontal surface in Tunisia and the Netherlands in the course of one day/night cycle. The light intensity is derived from the light model as described in Appendix B. No cloud cover is assumed in Tunisia while the light intensity is evenly reduced by 40% in the Netherlands to simulate the cloud cover.

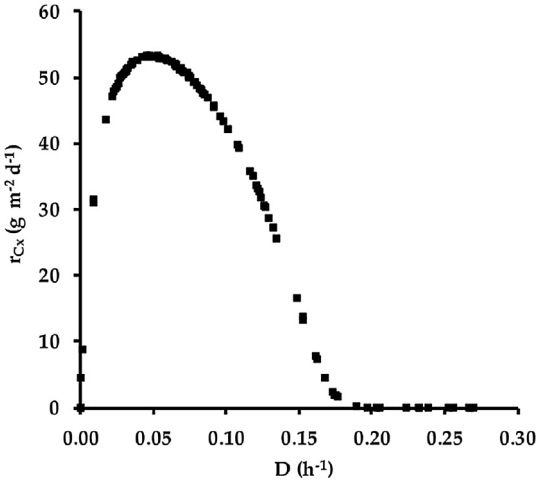

Fig. A3. Areal productivity versus dilution rate of a mutant that is 80% reduced in a_X simulated for cultivation in Tunisia. Dilution only occurred during light hours at a constant rate. During the night, there was no dilution. The daily light intensity was 55.8 mol$_{ph}$ m^{-2}d^{-1}.

the light intensity hitting the culture surface according to Fresnel's equations:

$$I_{ph,0} = \boldsymbol{I_{ph,0,i}} - \frac{1}{2} \cdot \left(\boldsymbol{R_s} + \boldsymbol{R_p}\right) \cdot \boldsymbol{I_{ph,0,i}} \quad \text{(A16)}$$

with the reflectivity of light polarized in the plane of incidence $R_s = \left(\frac{n_{air} \cdot \cos\theta_z' - n_{water} \cdot \cos\theta_z}{n_{air} \cdot \cos\theta_z' + n_{water} \cdot \cos\theta_z}\right)^2$ and perpendicular to the plane of incidence $R_p = \left(\frac{n_{water} \cdot \cos\theta_z' - n_{air} \cdot \cos\theta_z}{n_{water} \cdot \cos\theta_z' + n_{air} \cdot \cos\theta_z}\right)^2$.

Appendix C. : Light patterns

The irradiance and the light angle were simulated for a sunny location (Sidi Bou Said, Tunisia) and a location with a higher cloudage (De Bilt, the Netherlands). Measurements showed a global insolation of 16.67 MJ m^{-2} d^{-1} in mid-July (1971–1986) in the Netherlands (Velds et al., 1992). This insolation corresponds to 62% of the predicted insolation under a clear sky. Compared to that, in Tunisia, the average insolation in July (>10 years) is significantly higher (26.64 MJ m^{-2} d^{-1} over >10 years) (Alnaser et al., 2004). This value is 5% lower than the predicted insolation in Tunisia. While the low cloudage in Tunisia was neglected in the simulations, a constant cloudage of 40% was assumed in the Netherlands. All light including the diffuse part was assumed to be direct to simplify the simulations. The resulting light patterns for the chosen summer day in July that was used in all simulations are presented in Fig. A2.

Appendix D. : Dilution optimization procedure

The dilution rate was separately optimized for the areal biomass productivity of each strain. The optimization of the constant dilution rate during the day was performed employing a controlled random search algorithm. The boundaries for the dilution rate were set to zero and the maximum growth rate to (0.27 h^{-1}). Within these boundaries, 50 random values for the dilution rate were drawn. A cultivation period of 15 days was simulated for each dilution rate. The average productivity was calculated for the last 24 h. All dilution rates and the corresponding productivities were recorded on a list with 50 data pairs. Stepwise, the dilution rates and productivities in the list were replaced with data pairs containing higher productivities. First, four dilution rates ($D_{r,1}$ to $D_{r,4}$) were randomly drawn and combined with the last dilution rate in the list (D_{end}) to return a new value (D_{new}, Eq. (A17)).

$$D_{new} = 2 \cdot \left(\frac{\sum_{i=1}^{i=4} D_{r,i}}{4}\right) - D_{end} \quad \text{(A17)}$$

Second, the same simulation as described above followed for the new dilution rate if the boundary conditions were still met. Otherwise, a new value was generated and the simulation was performed with the first value within the boundary conditions. Third, the productivity resulting from this simulation was compared to the lowest productivity in the list. The data pair with the lowest productivity was replaced if it the new productivity was higher. The new data pair was discarded if the new productivity was lower. By repeating this pattern, a dense data set around the optimal dilution rate was generated (See Fig. A3 for an example). The dilution rate corresponding to the maximum areal biomass productivity was used for all simulations with the respective strain.

Appendix E. : Model variables and parameters

See Table A1 and Table A2 .

Appendix F. Supplementary data

Supplementary data associated with this article can be found, in the online version, at http://dx.doi.org/10.1016/j.jbiotec.2016.10.009.

Table A1
Overview of location and time dependent variables and parameters used for the derivation of the light pattern.

Symbol	Description	Unit
NL	Location in the Netherlands, town: De Bilt	–
TU	Location in North Tunisia, town: Sidi Bou Said	–
t	Cultivation time with t_0 = 8am local solar time	h
d	Number of the day in the year	–
t_{solar}	Local solar time, position of the sun is highest at 0° or t_{solar} = 12am	h
P_{light}	Duration of the light period in one day/night cycle	h
PAR	Photosynthetic active radiation (spectrum of 400 to 700 nm)	–
λ	Wavelength	nm
E_e	Solar power on the horizontal earth surface neglecting effects of the atmosphere	$\frac{W}{m^2}$
G_{clear}	Solar power reaching the earth on a specific location including effects of the atmosphere	$\frac{W}{m^2}$
$I_{ph,0,i}$	Global light intensity that hits the earth surface before light is reflected	$\frac{mol_{ph}}{m^2 \cdot s}$
$I_{ph,0}$	Global light intensity on the horizontal culture surface that is transmitted into the culture according to Fresnel's equations	$\frac{mol_{ph}}{m^2 \cdot s}$
$I_{ph,0,r}$	Global light intensity that is reflected at the reactor surface.	$\frac{mol_{ph}}{m^2 \cdot s}$
$I_{ph,\lambda,down}(z)$	Wavelength-specific light intensity at every position z without the addition of light that is reflected at the pond floor.	$\frac{mol_{ph}}{m^2 \cdot s}$
$I_{ph,\lambda,up}(z)$	Wavelength-specific light intensity at every position z limited to light that is reflected at the bottom of the pond floor.	$\frac{mol_{ph}}{m^2 \cdot s}$
$\frac{1}{\cos(\theta_z')}$	Enhancement factor correlating the light path to the reactor depth	–
θ_z	Zenith angle, the angle between sunrays and the perpendicular to the earth surface	°
θ_z'	Refracted zenith angle, the zenith angle after refraction according to Snell's law	°
$\theta'_{z,diff}$	Refracted zenith angle, the zenith angle after refraction at the bottom of the pond photobioreactor.	
δ	Solar declination, tilt of the earth relative to the sun	°
$\bar{R}$	Average distance between the earth and sun over the year	–
R	Average distance between the earth and sun over the day	–
R_s	Reflectivity of light polarized in the plane of incidence	–
R_p	Reflectivity of light polarized perpendicular to the plane of incidence	–

Parameter	Description	Value	Unit	Ref.
S_0	Solar constant	1367.0	$\frac{W}{m^2}$	Fröhlich and Brusa (2016)
T_L	Turbidity coefficient by Linke, TU: averaged from daily values in mid of July in, NL: July 15th in De Bilt	5.9 [NL] 5.5 [TU]	–	Velds et al. (1992), Chaâbane et al. (2004)
ϕ	Latitude	52.117 [NL]36.867 [TU]	–	
f_R	Fraction of reflected light of reflective ground cover.	0.8	–	Meinhold et al. (2010)

Table A2
Overview of time dependent variables describing the sugar production rate and carbon partitioning and the productivity. The index i refers to the application of the parameter on both strains in the reactor, the mutant and the wild type.

Symbol	Description	Unit
qph_i	Biomass specific photon absorption rate	$\frac{mol_{ph}}{mol_{X'} \cdot s}$
q_{S_i}	Biomass specific sugar production rate	$\frac{mol_S}{mol_{X'} \cdot s}$
$\frac{dX'_i}{dt}$	Accumulation rate of functional biomass	$\frac{mol_{X'}}{s \cdot m^3}$
$\frac{dS_i}{dt}$	Accumulation rate of sugar stored as starch	$\frac{mol_S}{s \cdot m^3}$
Cx_i	Total molar biomass concentration in the reactor (normalized to 1 mol carbon)	$\frac{mol_{Cx}}{m^3}$
$Y_{Cx/ph}$	The biomass yield on incident light energy	$\frac{g_{Cx}}{mol_{ph}}$
X'_i	Molar concentration of functional biomass (normalized to 1 mol carbon)	$\frac{mol_{X'}}{m^3}$
S_i	Molar concentration of sugar stored as starch (normalized to 1 mol carbon)	$\frac{mol_S}{m^3}$
$x_{S,i}$	Molar fraction of sugar in the total biomass	$\frac{mol_S}{mol_{Cx}}$
r_{Cx}	Areal biomass productivity	$\frac{g_{Cx}}{m^2 \cdot d}$

Table A3
Overview of model parameters related to the organism, substances, or the light and the reactor. Organism specific parameters are either originating from C. sorokiniana or generally assumed for green algae. The index i refers to the application of the parameter on both strains in the reactor, the mutant and the wild type.

Parameter	Value	Unit	Description	Origin	Ref.
μ_m	0.27	h^{-1}	Maximum biomass specific growth rate[a]	*C. sorokiniana*	(Blanken et al., 2016)
m_S	$2.69 \cdot 10^{-6}$	$\frac{mol_S}{mol_{X'} \cdot s}$	Biomass specific maintenance rate normalized to functional biomass	*C. sorokiniana*	(Blanken et al., 2016)
$m_{X'}$	$2.41 \cdot 10^{-6}$	$\frac{mol_{X'}}{mol_{X'} \cdot s}$	Biomass specific maintenance rate normalized to functional biomass		(Blanken et al., 2016)
$Y_{X'/S}$	0.56	$\frac{mol_{X'}}{mol_S}$	Functional biomass yield on 3-carbon sugar using ammonia as nitrogen source	*C. sorokiniana*	(Blanken et al., 2016)
q_S^{max}	$1.21 \cdot 10^{-4}$	$\frac{mol_S}{mol_{X'} \cdot s}$	Maximum functional biomass specific sugar production rate, $\mu_m = \left(q_S^{max} - m_S\right) \cdot Y_{X'/S}$	*C. sorokiniana*	
$x_{S,min,i}$	0.07	$\frac{mol_S}{mol_{Cx}}$	Minimum sugar content 0.08 $\frac{g_S}{g_{Cx}}$ in total biomass	*C. sorokiniana*	(Blanken et al., 2016)

Table A3 (*Continued*)

Parameter	Value	Unit	Description	Origin	Ref.
$\mathbf{a}_{X',\lambda,i}$	see Table S1	$\frac{m^2}{mol_{X'} \cdot nm}$	Wavelength-specific absorption cross section, value for mutant as a percentage of wild type	*C. sorokiniana*	
$Y_{S/ph,m,\lambda}$	see Table S1	$\frac{mol_S}{mol_{ph} \cdot nm}$	Maximum wavelength dependent yield of sugar on photons	*Cyanobacteria, green algae*	
$M_{X'}$	24	$\frac{g_{X'}}{mol_{X'}}$	Biomass dry weight to C-mol conversion factor for functional biomass.		
M_S	27	$\frac{gs}{mol_S}$	Molecular weight of a polysaccharides of glucose normalized to 1 mol carbon		(GESTIS-Stoffdatenbank, 2015)
n_{air}	1.00	–	Refractive index of air		(Denny, 1993)
n_{water}	1.33	–	Refractive index of water		(Denny, 1993)
z		m	Position in the reactor		
d_R	0.20	m	Reactor depth		
$E_{n,\lambda}$	see Table S1	nm^{-1}	Relative light distribution in the spectrum of 400–700 nm		

[a] The value of $m_{X'}$ was estimated based on m_S and the degree of reduction (γ) of microalgal biomass and sugar (CH_2O): $m_{X'} = m_S \cdot \gamma_{sugar}/\gamma_{biomass}$.

References

Acién Fernández, F., García Camacho, F., Sánchez Pérez, J., Fernández Sevilla, J., Molina Grima, E., 1998. Modeling of biomass productivity in tubular photobioreactors for microalgal cultures: effects of dilution rate, tube diameter, and solar irradiance. Biotechnol. Bioeng. 58, 605–616.

Agostoni, M., Lucker, B.F., Smith, M.A., Kanazawa, A., Blanchard, G.J., Kramer, D.M., Montgomery, B.L., 2016. Competition-based phenotyping reveals a fitness cost for maintaining phycobilisomes under fluctuating light in the cyanobacterium *Fremyella diplosiphon*. Algal Res. 15, 110–119.

Alnaser, W.E., Eliagoubi, B., Al-Kalak, A., Trabelsi, H., Al-Maalej, M., El-Sayed, H.M., Alloush, M., 2004. First solar radiation atlas for the Arab world. Renew. Energy 29, 1085–1107.

Blanken, W., Postma, P.R., de Winter, L., Wijffels, R.H., Janssen, M., 2016. Predicting microalgae growth. Algal Res. 14, 28–38.

Cazzaniga, S., Dall'Osto, L., Szaub, J., Scibilia, L., Ballottari, M., Purton, S., Bassi, R., 2014. Domestication of the green alga *Chlorella sorokiniana*: reduction of antenna size improves light-use efficiency in a photobioreactor. Biotechnol. Biofuels 7, 157.

Chaâbane, M., Masmoudi, M., Medhioub, K., 2004. Determination of Linke turbidity factor from solar radiation measurement in northern Tunisia. Renew. Energy 29, 2065–2076.

Cooper, P.I., 1969. The absorption of radiation in solar stills. Sol. Energy 12, 333–346.

Cornet, J.F., Dussap, C.G., 2009. A simple and reliable formula for assessment of maximum volumetric productivities in photobioreactors. Biotechnol. Progr. 25, 424–435.

Cuaresma, M., Janssen, M., Vílchez, C., Wijffels, R.H., 2011. Horizontal or vertical photobioreactors? How to improve microalgae photosynthetic efficiency. Bioresour. Technol. 102, 5129–5137.

Denny, M.W., 1993. Air and Water: the Biology and Physics of Life's Media. Princeton University Press.

Duffie, J.A., Beckman, W.A., 2016. Solar Engineering of Thermal Processes. Wiley New York etc., pp. 1980.

Fábregas, J., Maseda, A., Domínguez, A., Ferreira, M., Otero, A., 2002. Changes in the cell composition of the marine microalga, *Nannochloropsis gaditana*, during a light: dark cycle. Biotechnol. Lett. 24, 1699–1703.

Flynn, K.J., Greenwell, H.C., Lovitt, R.W., Shields, R.J., 2010. Selection for fitness at the individual or population levels: modelling effects of genetic modifications in microalgae on productivity and environmental safety. J. Theor. Biol. 263, 269–280.

Flynn, K., Mitra, A., Greenwell, H., Sui, J., 2013. Monster potential meets potential monster: pros and cons of deploying genetically modified microalgae for biofuels production. Interface Focus 3, 20120037.

Flynn, K.J., 2001. A mechanistic model for describing dynamic multi-nutrient light, temperature interactions in phytoplankton. J. Plankton Res. 23, 977–997.

Formighieri, C., Franck, F., Bassi, R., 2012. Regulation of the pigment optical density of an algal cell: filling the gap between photosynthetic productivity in the laboratory and in mass culture. J. Biotechnol. 162, 115–123.

Fröhlich, C., Brusa, R., 2016. Solar Radiation and Its Variation in Time, Physics of Solar Variations. Springer1981, pp. 209–215.

Franco, M.C., Buffing, M.F., Janssen, M., Lobato, C.V., Wijffels, R.H., 2012. Performance of *Chlorella sorokiniana* under simulated extreme winter conditions. J. Appl. Phycol. 24, 693–699.

IFA, GESTIS-Stoffdatenbank (accessed 09.15.15).

Geider, R., MacIntyre, H., Kana, T., 1997. Dynamic model of phytoplankton growth and acclimation: responses of the balanced growth rate and the chlorophyll *a*: carbon ratio to light, nutrient-limitation and temperature. Mar. Ecol. Prog. Ser. 148, 187–200.

Gibson, R., Atkinson, R., Gordon, J., 2008. Use abuse, misconceptions and insights from quota models—the droop cell quota model 40 years on. Oceanogr. Mar. Biol.: Annu. Rev. 46, 1–23.

Glick, R.E., Melis, A., 1988. Minimum photosynthetic unit size in system I and system II of barley chloroplasts. Biochim. Biophys. Acta (BBA)-Bioenerg. 934, 151–155.

Goldstein, D.H., 2010. Polarized Light. CRC Pres.

Hobson, P., 1969. Growth of mixed cultures and their biological control. Microb. Growth, 43–64.

Huesemann, M., Crowe, B., Waller, P., Chavis, A., Hobbs, S., Edmundson, S., Wigmosta, M., 2016. A validated model to predict microalgae growth in outdoor pond cultures subjected to fluctuating light intensities and water temperatures. Algal Res. 13, 195–206.

Huisman, J., Jonker, R.R., Zonneveld, C., Weissing, F.J., 1999. Competition for light between phytoplankton species: experimental tests of mechanistic theory. Ecology 80, 211–222.

Jassby, A.D., Platt, T., 1976. Mathematical formulation of the relationship between photosynthesis and light for phytoplankton. Limnol. Oceanogr. 21, 540–547.

Kasten, F., Czeplak, G., 1980. Solar and terrestrial radiation dependent on the amount and type of cloud. Sol. Energy 24, 177–189.

Klein, U., 1987. Intracellular carbon partitioning in *Chlamydomonas reinhardtii*. Plant Physiol. 85, 892–897.

Kliphuis, A.M., de Winter, L., Vejrazka, C., Martens, D.E., Janssen, M., Wijffels, R.H., 2010. Photosynthetic efficiency of *Chlorella sorokiniana* in a turbulently mixed short light-path photobioreactor. Biotechnol. Prog. 26, 687–696.

Kwon, J.-H., Bernát, G., Wagner, H., Rögner, M., Rexroth, S., 2013. Reduced light-harvesting antenna: consequences on cyanobacterial metabolism and photosynthetic productivity. Algal Res. 2, 188–195.

Lacour, T., Sciandra, A., Talec, A., Mayzaud, P., Bernard, O., 2012. Diel variations of carbohydrates and neutral lipids in nitrogen-sufficient and nitrogen-starved cyclostat cultures of *Isochrysis* sp. 1. J. Phycol. 48, 966–975.

Lee, E., Pruvost, J., He, X., Munipalli, R., Pilon, L., 2014. Design tool and guidelines for outdoor photobioreactors. Chem. Eng. Sci. 106, 18–29.

Meinhold, T., Richters, J.-P., Damerow, L., Blanke, M., 2010. Optical properties of reflection ground covers with potential for enhancing fruit colouration. Biosyst. Eng. 107, 155–160.

Melis, A., Neidhardt, J., Benemann, J.R., 1998. *Dunaliella salina* (Chlorophyta) with small chlorophyll antenna sizes exhibit higher photosynthetic productivities and photon use efficiencies than normally pigmented cells. J. Appl. Phycol. 10, 515–525.

Mitra, M., Melis, A., 2008. Optical properties of microalgae for enhanced biofuels production. Opt. Express 16, 21807–21820.

Mooij, P.R., Stouten, G.R., van Loosdrecht, M.C., Kleerebezem, R., 2015. Ecology-based selective environments as solution to contamination in microalgal cultivation. Curr. Opin. Biotechnol. 33, 46–51.

Mussgnug, J.H., Thomas-Hall, S., Rupprecht, J., Foo, A., Klassen, V., McDowall, A., Schenk, P.M., Kruse, O., Hankamer, B., 2007a. Engineering photosynthetic light capture: impacts on improved solar energy to biomass conversion. Plant Biotechnol. J. 5, 802–814.

Mussgnug, J.H., Thomas-Hall, S., Rupprecht, J., Foo, A., Klassen, V., McDowall, A., Schenk, P.M., Kruse, O., Hankamer, B., 2007b. Engineering photosynthetic light capture: impacts on improved solar energy to biomass conversion. Plant Biotechnol. J. 5, 802–814.

Oey, M., Ross, I.L., Stephens, E., Steinbeck, J., Wolf, J., Radzun, K.A., Kügler, J., Ringsmuth, A.K., Kruse, O., Hankamer, B., 2013. RNAi knock-down of LHCBM1 2 and 3 increases photosynthetic H2 production efficiency of the green alga *Chlamydomonas reinhardtii*. PLoS One 8, e61375.

Ogbonna, J.C., Tanaka, H., 1996. Night biomass loss and changes in biochemical composition of cells during light/dark cyclic culture of *Chlorella pyrenoidosa*. J. Ferment. Bioeng. 82, 558–564.

Ort, D.R., Zhu, X., Melis, A., 2011. Optimizing antenna size to maximize photosynthetic efficiency. Plant Physiol. 155, 79–85.
Perrine, Z., Negi, S., Sayre, R.T., 2012. Optimization of photosynthetic light energy utilization by microalgae. Algal Res. 1, 134–142.
Pirt, S., 1965. The maintenance energy of bacteria in growing cultures. Proc. R. Soc. Lond. B: Biol. Sci. 163, 224–231.
Post, A.F., loogman, J.G., Mur, L.R., 1985. Regulation of growth and photosynthesis by *Oscillatoria agardhii* grown with a light/dark cycle. FEMS Microbiol. Lett. 31, 97–102.
Pruvost, J., Cornet, J., Le Borgne, F., Goetz, V., Legrand, J., 2015. Theoretical investigation of microalgae culture in the light changing conditions of solar photobioreactor production and comparison with cyanobacteria. Algal Res. 10, 87–99.
Quinn, J., De Winter, L., Bradley, T., 2011. Microalgae bulk growth model with application to industrial scale systems. Bioresour. Technol. 102, 5083–5092.
Rosenberg, J.N., Kobayashi, N., Barnes, A., Noel, E.A., Betenbaugh, M.J., Oyler, G.A., 2014. Comparative analyses of three *Chlorella species* in response to light and sugar reveal distinctive lipid accumulation patterns in the microalga *C. sorokiniana*. PLoS One 9, e92460.
Sharkey, T.D., 2015. Understanding carbon partitioning and its role in determining plant growth. Plant Cell Environ.
Sonnewald, U., Kossmann, J., 2013. Starches—from current models to genetic engineering. Plant Biotechnol. J. 11, 223–232.
Sukenik, A., Carmeli, Y., 1990. Lipid synthesis and fatty acid composition in *Nannochloropsis* sp. (Eustigmatophyceae grown in a light-dark cycle1. J. Phycol. 26, 463–469.
Takache, H., Pruvost, J., Cornet, J.F., 2012. Kinetic modeling of the photosynthetic growth of *Chlamydomonas reinhardtii* in a photobioreactor. Biotechnol. Prog. 28, 681–692.
Velds, C.A., Van der Hoeven, P., Koopstra, J., Raaf, W., Slob, W., 1992. Zonnestraling in nederland. Thieme Baarn.
Zhu, X.-G., Long, S.P., Ort, D.R., 2010. Improving photosynthetic efficiency for greater yield. Annu. Rev. Plant Biol. 61, 235–261.
Zijffers, J.-W.F., Schippers, K.J., Zheng, K., Janssen, M., Tramper, J., Wijffels, R.H., 2010. Maximum photosynthetic yield of green microalgae in photobioreactors. Mar. Biotechnol. 12, 708–718.
de Mooij, T., Janssen, M., Cerezo-Chinarro, O., Mussgnug, J.H., Kruse, O., Ballottari, M., Bassi, R., Bujaldon, S., Wollman, F.-A., Wijffels, R.H., 2014. Antenna size reduction as a strategy to increase biomass productivity: a great potential not yet realized. J. Appl. Phycol., 1–15.